



Performance Analysis of Varying Tool Pin Profile on Friction Stir Welded 2050-T84Al-Cu-Li Alloy Plates

Sanjeev Kumar, Sujeet Kumar Chaubey, Durjyodhan Sethi, Subhash Chandra Saha, and Barnik Saha Roy

Submitted: 22 August 2020 / Revised: 31 July 2021 / Accepted: 15 September 2021 / Published online: 25 October 2021

In this paper, different tool pin profiles, namely taper-threaded, triangular, and hybrid are used to join 5-mm-thick 2050-T84 Al-Cu-Li alloy by friction-stir-welding. The experiments were conducted using a one-variable-at-a-time approach by varying the geometry of tool pin profile and kept constant values of tool rotational speed, tool traverse speed, and tool tilt angle as 1400 rpm, 180 mm/min, and 2°, respectively. The objectives of this paper are to determine the effects of varying tool pin profile on force–torque behavior, microstructure, grain size distribution, tensile properties, and mode of tensile failure. It was observed that the hybrid tool produced less flash, less vertical downward force (14340.49N), low average grain size (11.27 μm) in the nugget zone, and larger weld bead area along with higher tensile strength (418.98 MPa), joint efficiency (78.44%), and micro-hardness (147HV_{0.1}) when compared to other tools. The fractography analyses were performed using field-emission scanning electron microscope and observed ductile mode of failure for all friction stir-welded joints.

Keywords 2050-T84Al-Cu-Li alloy, friction stir welding, grain size, microstructure, mechanical properties, tool pin profile

1. Introduction

Increase in demand of light-weighted and high strength materials in aerospace, automotive, and defense industries alongwith less fuel consumption has pressurized for innovation of novel material (Ref 1) and to meet the required demands, copper (high) and lithium ($0.6 < \text{Li} < 1.5$ %weight) in the form of 2050-T84 Al-Li alloy plays a vital role due to its excellent mechanical properties (Ref 2). It exhibits properties like low density, high strength, high stiffness to density ratio, higher corrosion resistance, improved fatigue toughness, and resistance to crack propagation with excellent damage tolerance (Ref 3, 4). 2050-T84 Al-Li alloy replaces the legacy of 7050-T74 alloy by reduction in stress concentration (46%), enhanced fatigue life (25%), improved stiffness (7%), toughness (6%), mechanical strength (8%), and reduced density (4%). On comparing the legacy of 2219-T87 with AA2050-T84, the latter exhibits 34% better yield strength, increases the elongation by 17%, reduces the density by 5% (Ref 5). 2050-T84 Al-Li alloy is extensively used in the frame, bulkhead, upper wing cover, spars, ribs, and other internal structures of aircraft and replaces AA 2xxx and 7xxx series of aluminum alloys. 2050-T84 Al-Li alloy is also used in the cryogenic propellant tank of launch

vehicle spacecraft (Ref 6, 7). 1% weight of Li added in Al alloy decreases the density by 3%, increases Young's modulus by 6%, and improves the fatigue crack growth resistance (Ref 8–10). There are three types of strengthening precipitate, namely Ω (Al_2Cu), T1 (Al_2CuLi), and δ' (Al_3Li), revealed in Al-Cu-Li alloys which depends upon the % weight of Li and Cu in alloys. The weight percentage of Li between 0.6-1.5 in Al-Cu-Li alloys exhibits Ω (Al_2Cu) and T1 (Al_2CuLi) phase, respectively. The appearance of the T1 phase in AA2050 alloy provides the most effective strengthening phase, which was observed as a very thin-shaped particle on the {111} plane (Ref 11). Whereas when more than 1.5% weight of Li is added in an alloy, less strengthening precipitate like δ' phase (Al_3Li), the θ' phase (Al_2Cu), T2 ($\text{Al}_5\text{Li}_3\text{Cu}$), and TB ($\text{Al}_7\text{Cu}_4\text{Li}$) was observed in Al-Li alloy (Ref 12-14).

2050-T84 Al-Li alloy is prone to weak welding joints with conventional welding processes due to several defects like porosity, oxide layers formation, and cracks. The traditional welding process causes the loss of the lithium element (Li) in 2050-T84 Al-Li alloy due to the low melting point of lithium. In 1991, The Welding Institute (TWI) invented an environment-friendly, energy-efficient, and the solid-state joining technique known as FSW to eliminate several limitations of conventional welding 2050-T84 Al-Li alloy and to produce improved joint efficiency alongwith the utilization ratio in aerospace and mechanical properties (Ref 15). There are four stages in FSW– (i) plunge stage (rotating tool gradually penetrates into the workpiece till shoulder touches the surface of workpiece), (ii) dwell stage (the tool rotate continuously till material gets softened around the tool), (iii) welding stage (tool moves along the joint line for joining the material), and (iv) cooling stage (after welding the tool is pulled out from the workpiece which results in the decrease in the temperature of the joint) (Ref 16). During FSW process, a non-consumable rotating tool was used to join the material 2050-T84 Al-Cu-Li alloys [the tool pin plunged into the workpiece and shoulder which attributed the workpiece surface to generate the frictional heat followed by input process parameters (rotating speed, traverse speed, tilt angle, plunge depth, tool pin profile, and materials type)]

Sanjeev Kumar, Durjyodhan Sethi, Subhash Chandra Saha, and Barnik Saha Roy, Department of Mechanical Engineering, National Institute of Technology Agartala, Bajrala, Jirania 799046 West Tripura, India; and Sujeet Kumar Chaubey, Department of Mechanical and Industrial Engineering Technology, University of Johannesburg, Doornfontein 2028, South Africa. Contact e-mail: placid.san@gmail.com.

without melting the workpiece material. The tool pin generates 15% of the total heat generated and affects the intermixing pattern of plasticized material and flows toward the side from the advancing side (AS) to the retreating side (RS) (Ref 17).

Several research papers are available in the literature on aspects of different tool pin profiles on the microstructure and mechanical-properties of Al alloy. Few works are cited in this paragraph. Leon et al. (Ref 18) revealed that the hexagonal tool generates higher heat when compared to the triangular tool at a higher shoulder cone angle (4.5°) and lower pin cone angle (5°), due to the number of sides of the tool which was responsible for the flow rate of plasticized material underneath the shoulder and around the tool. Ugender et al. (Ref 19) reported that the taper threaded profile tool pin provides higher mechanical properties (tensile strength and the micro-hardness) than other tool profiles such as straight cylindrical profile, conical profile, and threaded conical profile. The triangular pin profile is superior to the threaded circular profile pin in terms of mechanical properties and joint efficiency of FSW welded AA5083 alloy plates at lower traverse speed (Ref 20). Elangovan et al. (Ref 21) reported that the square profile tool pin has higher tensile properties at axial force 7KN than the other tool pin profile. Palanivel et al. (Ref 22) also observed similar observations at axial force 1.5 tonnes using the different profile tool pin. Budin et al. (Ref 23) have reported that higher tensile strength can be achieved using a taper profile tool pin compared to the triangular and cylindrical profile tool pin. However, Rao et al. (Ref 24) recommended that the hexagonal tool pin profile has superior mechanical properties than other tool profiles, namely conical, square, triangular, and the pentagonal tool pin profile. Moradi et al. (Ref 25) found experimentally that the triangle pin profile has a higher hardness (TMAZ) and tensile properties than the square pin profile. Singh et al. (Ref 26) conferred that a straight cylinder threaded tool provides defects-free and smooth joint compared to the threaded profile tool pin. Elangovan et al. (Ref 27) observed that the square tool pin profile revealed better mechanical properties than other tools (straight cylindrical, conical, threaded cylindrical, triangular) at 1200 rpm. Singh et al. (Ref 28) joined AA 2024 plates with various tool pin profiles (conical, pedal, threaded cylindrical, triangular, square, and pentagonal) and found that a square tool pin profile produced the maximum tensile strength and joint efficiency. Dawood et al. (Ref 29) reported that the better mechanical-properties could be achieved using the triangular profile tool pin and observed the ductile mode of fracture by the triangular profile tool pin. Shalin et al. observed that the taper pin profile provides greater strength than the cylindrical pin and square tool pin at 2750 rpm and 15mm/min of FSWed 6061 alloys (Ref 30). Darmadi et al. used three different tool pins (circular, square, and triangular) to make single and double side FSW joints of 6061 alloys and observed that the triangular tool has superior mechanical qualities compared to the square and circular tools. The double side FSW joint has superior joint quality than the single side FSW joint (Ref 31).

The above conclusions from the past works significantly revealed the importance of different tool profiles that affect the joined material's microstructure and tensile properties. There is no work done on welding of 2050-T84 Al-Li alloy by different tool profiles (hybrid) in FSW to the best knowledge of authors. The present research work focused on determining the consequence of the various pin profile on FSW of 2050-T84 Al-Cu-Li alloy. In the current work, the 2050-T84 Al-Li alloy plate

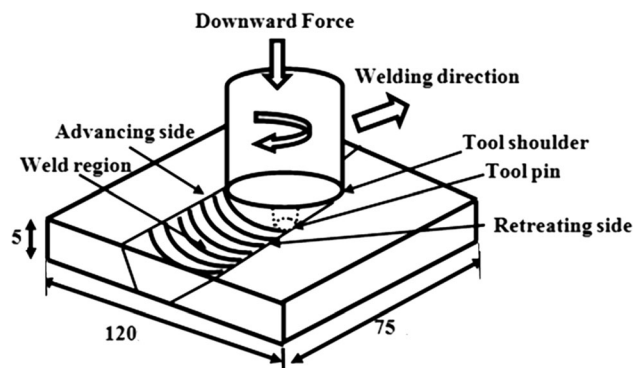


Fig. 1 Specifications of prepared samples made of 2050-T84 Al-Li alloy for FSW

having 5 mm thickness was welded by FSW using different tool profiles at constant tool rotational speed (TRS), tool traverse speed (TTS), and tool tilt angle (TTA). An approach toward the effect of different tool pin profiles on force and torque has also been discussed. The microstructural examination and tensile properties of the friction stir-welded 2050-T84 Al-Cu-Li alloy was also performed to determine the welded quality.

2. Experimental Procedure

A rectangular plate of base material 2050-T84 Al-Li alloy (obtained from GR Metalloys Private Limited, Ahmedabad, India) having the dimension of 75 mm length, 60 mm width and 5 mm thickness was used for welding by a 3T FSW machine (Model No. WS005, three tonnes capacity, supplied by Eta Technology Private Limited, Bangalore, India) parallel to the rolling direction in square butt configuration as shown in Fig. 1. The chemical composition and tensile properties of the parent material are illustrated in Table 1. The non-consumable rotating tool is used in FSW, which was made of H13 steel. A Concave shape shoulder has been used in all the tools for the welding. The concave shoulder restricts the extruded material from moving sideways and applies the downward force on displaced materials thereby creating a pressing action on plasticized material rear the probe. The different profile tool pins, namely taper threaded, triangular, and hybrid profile tool pin (Fig. 2), were used for experimentation at constant TRS (i.e., 1400rpm), TTS (i.e., 180mm/min.) and TTA (i.e., 2°). A set of variable parameters (TRS- 600, 1000, 1400, 1800 and TTS- 60, 120, 180, 240mm/min) were used to perform experiment by taper threaded tool pin and result showing optimum mechanical properties was selected for further experimental work. The hybrid tool pin profile (a combination of taper threaded and triangular) was manufactured so that the threaded taper profile is located in the base and the triangular profile on the top portion of the tool for better mixing and flowability of the material during FSW. The tool tip and bottom diameter of the taper threaded tool are 3 and 5 mm, respectively. The tool pin height and concave angle (angle between the shoulder surface and tool pin base) were kept constant as 4.8 mm and 5° , respectively. The shoulder surface's concavity acts as a reservoir that collects the displaced material from the tool pin and forges the material after the tool. As far as the length is concerned, one side of the triangular pin measured 4 mm. The apex part of the hybrid tool is triangular with side

Table 1 Chemical composition and the tensile properties of 2050-T84 Al-Cu-Li alloy(Ref 10)

Chemical composition, Weight %							Tensile properties					
Cu	Li	Ag	Mg	Mn	Zn	Zr	Ti	Fe	Si	UTS, MPa	YS, MPa	%E
3.6	0.98	0.48	0.38	0.32	0.12	0.08	0.03	0.03	0.02	534.1	452.1	14.16

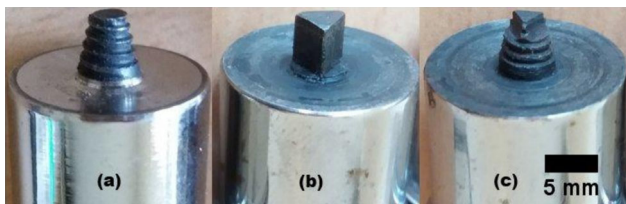


Fig. 2 Different types of tool pin profile used for experimentation; (a) the taper threaded (b) the triangular and (c) the hybrid tool pin profile

3mm and height 2.4 mm, whereas the bottom part of the tool is tapering with screw thread having height 2.4 mm, and its diameter vary from 3mm to 5mm. The plates should be free from dust, dirt, and foreign particles before welding. For each parameter, three experiments were performed for consistency and better accuracy in the results. Data (forces, and spindle torque) is accumulated from the data acquisition system (DAS), which is integrated in 3T FSW set-up to analyze the effect of considered parameters on microstructure and mechanical properties. Torque and forces are measured from the strain-gauge-based load cell, which was attached with DAS components (Transducer/sensor, signal conditioning and A/D converter) where noisy data is filtered and converted into digital form. These data are displayed by the Programmable logic controller (PLC), integrated with IPC and NI Lab view software.

For microstructure and mechanical property analysis (microstructure, grain size and tensile properties) of the welded joints, the samples were extracted in the transverse direction of the weld. The welded samples were polished by using different grade sized (400–2000) emery paper. Then the samples were cloth polished with hifin fluid and different graded (1, 0.5 and 0.25 μm) diamond paste. Finally it was etched using improved Keller's reagent (2 ml HNO_3 , 3ml HF, 6 ml HCl, and 89 ml H_2O) for the analysis of different zones in the welded sample. The microstructure was characterized with the help of the optical microscope (model- Leica DM2500, Germany). The average grain size was calculated through image-J software as per ASTM E 112-12. The three dog-bone shaped tensile specimens were prepared according to the ASTM-E8 guideline for tensile testing. Tensile tests were conducted on Instron-1195 at room temperature with a strain rate of 0.5mm min^{-1} . The Hardness of welded polished sample ($0.25\mu\text{m}$) was measured at mid-thickness in both direction (AS and RS) at 1 mm distance by the Vicker's hardness testing machine (Matsuzawa MMT-X Series) as per ASTM E384 with applying load 100gf for 10s. For fracture analysis, the advance side of the broken tensile specimens was selected to see the nature of the failure pattern with the help of Field Emission Scanning Electron Microscope (FE-SEM, sigma-300, Carl Zesis) images.

3. Results and Discussion

In this section, various aspects such as force and torque affected by different tool pin profiles at higher TRS, TTS, and TTA are described. The data (forces and torque) was composed in DAS and was analyzed through origin software alongwith appearance of the effect of different pin profile on weld bead surface. Further, the consequences of different tool pin on grain size distribution and counts in the weld nugget, microstructure, and tensile properties are also presented in this paper.

3.1 Force and Torque Analysis

The effect of different tool pin profiles, namely taper threaded, triangular, and hybrid pin profile on different forces (X and Z-force), and spindle torque, is shown in Fig. 3(a, b and c). The graphs of forces and torque have been plotted from the database recorded and saved in the DAS of FSW set up during FSW. It has been observed that the triangular pin profile has applies more force and torque during welding than the taper threaded and hybrid tool and shortly after achieving a dwell stage, the triangular tool pin broke. For this reason, the triangular pin profile showed an abrupt decrement in X-force and torque. These variations are shown in Fig. 3 (a and c). Generally, triangular tool pin generates more frictional heat due to the tool pin sides, which increase the surface contact with the workpiece. High traverse speed (180 mm/min) was applied during the experiment. Further, in welding stage, the triangular pin profile experienced more resisting force in the direction of welding, which reduced the tool pin's life, it may be due to one of the following reasons (Ref 18). The plasticized material is mixed properly by the taper threaded tool pin profile due to its geometrical structure (screw thread). The tool's concave shoulder feed the plasticized material which extruded during the tool's forward movement and flew outward by the tool pin. Before the end of the welding process, the material gets preheated due to the conduction process and the generation of higher frictional heat during FSW process may produce the stick slip phenomena which also affects the force–torque behavior. A similar trend is followed by the hybrid tool, but it shows a lower fluctuation in forces (X and Z) and spindle torque; it is shown in the respective graph. It may be due to the coupling of a triangular and tapered thread pin, which provides sufficient cooling time to promote the material's consolidation. It has also been observed that the weld bead appearance surface offers the same trend, which is concerned with tapering threaded tool profile.

3.2 Friction Stir Welded Surface and their Macrostructure

The weld bead appearance of the friction stir welded specimen with varying tool pin profile and their respective macrostructure are enlisted in Table 2. The tool geometry was configured according to various literature. Hou et al. (Ref 32)

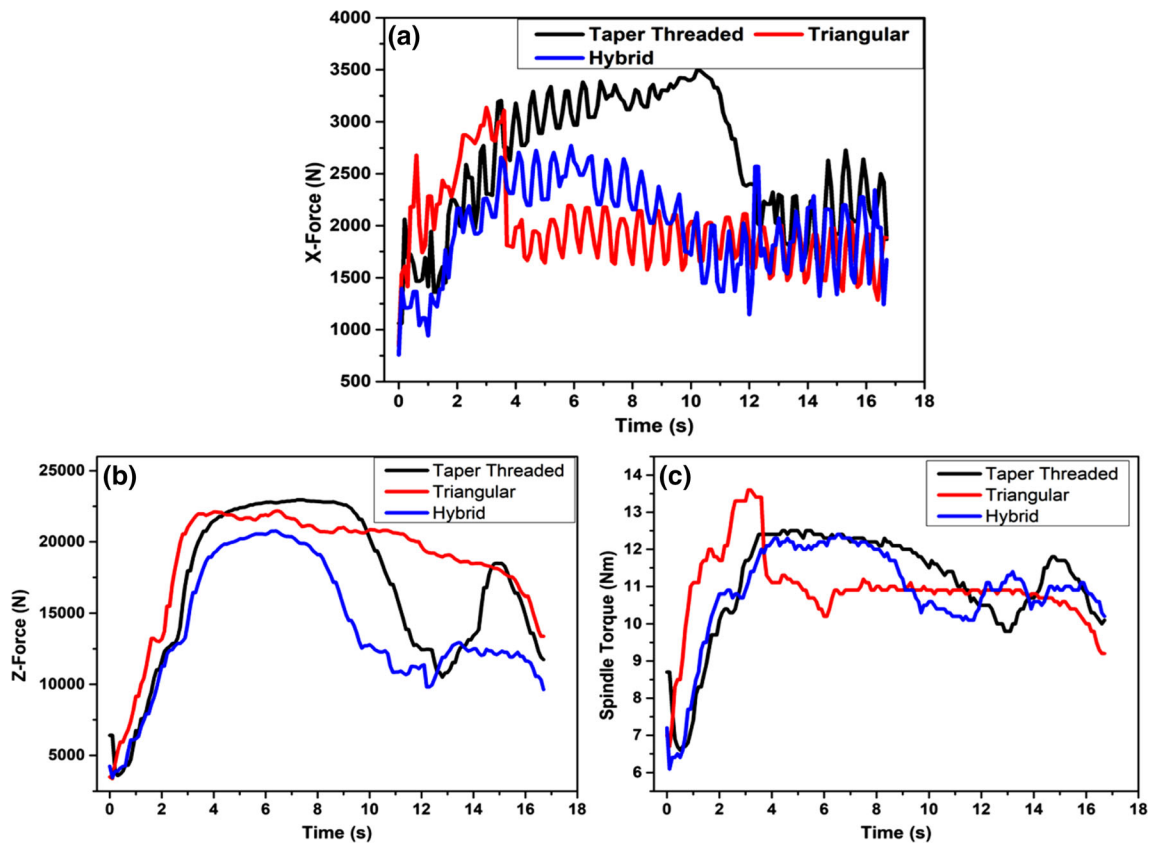
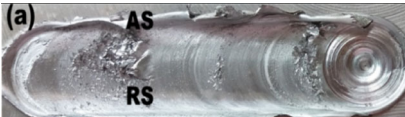







Fig. 3 Effect of the different tool pin profile on: (a) X-force (b) Z- force and (c) spindle torque with respect to time

Table 2 Weld bead appearance and macrostructure generated by different tool pin profile

Tool Profile	Weld Surface appearance	Macrostructure
Taper threaded		
triangular		
Hybrid		

proposed the shoulder diameter between the range of 16–18 mm, which produced defect-free joint. However, Khalilabad et al. (Ref 33) revealed that the shoulder diameter should be 2.2 times of workpiece thickness +7.3 mm for defect-free joint and

significant strengthening of the tool. A basin-shaped NZ macrostructure was observed for all welds. The smooth weld bead surface was observed by using hybrid tool and triangular tool as compared to the taper threaded tool. Eventhough the

triangular pin broke during welding and it is indicated in the red circle in Table 2(b). It may be due to the insufficient amount of heat generated which couldn't soften the plasticized material thereby generating high stress on the tool during welding. On account of tool geometry, the taper threaded produced sufficient amount of heat required for proper mixing of the plasticized material and formed concentrated tool tip area and higher tool pin base area as compare to triangular tool. Flash was seen on both the sides of the welded region, but the higher flash generation took place on the advance side. The hybrid pin profile generates less flash and provides excellent surface quality as compared to the taper threaded pin profile. The larger nugget area was observed in hybrid tool post welding, which may be probably due to tool pin structure (the higher swept volume of triangular pin profile, and taper threaded pin which provides the better mixing of the plasticized material and more incompressible flow of material in the pin region (Ref 31)). Macrostructure reveals that the bottom portion of NZ using triangular and hybrid tool is near about same but the NZ area varies due to difference in tool's structure. The red circle as shown in Table 2(b) shows the evidence of possible tool breakage of the triangular pin profiled tool. The possible reason for this may be due to insufficient amount of heat generated and high induced stress developed on the pin during welding. Macrostructure of hybrid tool appears combination of both taper threaded and triangular tool as it is shown in Table 2, in which the bottom part of the structure resembles with taper threaded and the upper part appear as same as triangular tool which can be seen very clearly in Table 2c.

3.3 Microstructural Analysis

The microstructure of the square butt welded 2050-T84 Al-Li alloy was analyzed with different tool pin profile. Defect-free (except triangular tool pin) joints were produced for all welds on similar parameters. Mainly three different microstructural zones were formed during FSW such as Nugget Zone (NZ), Thermo-Mechanical Affected Zone in advance side (TMAZ-AS), and retreating side (TMAZ-RS) and Heat-Affected Zone (HAZ). NZ and TMAZ (AS and RS) of welded samples and is shown in Fig. 4. An onion ring structure was observed within the stir zone of the triangular and hybrid tool (After diamond polishing). These are mainly generated due to suitable combinations of process parameters and tool profile that assists material movement in layers. On the AS, high strain shear bands generated by the tool pin extrudes the material on RS which initiates the formation of onion ring structure (Ref 34). On both side of the nugget zone, a definite pattern of flow of material on both the extremities (AS & RS) can be noticed. This is further augmented when hybrid tool is used. The stirring action of the tool influenced the movement of the material due to the optimal translational rate. The softening material moved from AS to RS, which may be one of the reasons for the formation of the onion ring in NZ (Ref 35).

The composition of constitute elements (Al, Li, Cu, Mg, etc.) of welded samples (2050-T84 Al-Li alloy) is revealed from FE-SEM/EDS (Energy dispersive spectroscopy) analysis. The constitute elements play the significant role like increased strengthening, decreased corrosion resistance and reinforced precipitate of the welded samples. The primary constitute particle (Cu) has been observed to play a significant role in strengthening of the alloy. The distribution of particles with the different tool pin is depicted in Fig. 5. The hybrid tool provides

well-mixed particle distribution in NZ as compared to the triangular and the taper threaded tool. However, the taper threaded tool mixed the material more finely than the triangular, it may be probably due to the presence of thread where the material is in contact with the tool more. The needle shaped particle was observed in the FE-SEM image (which was obtained in microstructural analysis after the welding by the triangular tool), the same is depicted in Fig. 5(a). Point EDS analysis at NZ with the respective FE-SEM image is depicted in Fig. 5(b). The percentage composition of constitute elements and EDS analysis of respective points shown in Fig. 5(c). From the EDS analysis, the lowest amount of copper (2.92% weight) was found in the welded sample with the triangular tool pin profile, while the highest (3.84% weight) was obtained from the hybrid tool pin profile. It may be due to the presence of intermetallic element of Cu in welded sample by using hybrid tool which is more and provide higher strength among all tools. The taper threaded tool pin profile revealed 3.57 % weight of copper in the welded sample, which (taper threaded tool pin) provides higher strength than the triangular pin.

After the sample was mirror polished and etched with modified Keller's solutions, the different shaped and sized grains of welded samples were observed in different zones. The grain size distribution in NZ by the different tools is shown in Fig. 6. The grain size (measured through the Image-J software) plays a significant role in improving mechanical properties. Three optical microstructures with clear grains were analyzed with similar magnification and scale to minimize the error and maintain consistency in the results. The fine equiaxed grains are observed in NZ due to the dynamic recrystallization after the FSW process is shown in Fig. 6. The triangular pin profile produced more elongated grain structure in NZ whereas the taper threaded pin profile produced less elongation but with more homogeneity. It has been observed that the grain size formed at the end of the triangular pin is less than that at the taper threaded, which contains a more uniform grain size in NZ. The hybrid tool pin profile has a smaller grain size but containing higher strength. The equation given by Hall-Petch indicates the same thing as in the equation (i). Every notation has a different meaning, such as " σ_y " denotes the Yield's Stress, " σ_0 " Material constant, " k " Strengthening coefficient, and " D " average grain size diameter (Ref 36, 37).

$$\sigma_y = \sigma_0 + \frac{k}{\sqrt{D}} \quad (\text{Eq 1})$$

The Hall-Petch relation (between the grain size diameter and Yield strength) of welded samples which was fabricated by different tool pin profile is shown in Fig. 7. The Yield strength of welded samples are increasing with decreasing grain size for all-welded samples. Further, based on linear fitting, the Y-intercepts (σ_0) and slope K were determined to be 293 and $1329.65\sqrt{\mu\text{m}}$ MPa. The Pearson correlation coefficient ($r = 0.99$) and r square= 0.97 , shows the stronger relationship between the yield strength and grain size of welded sample. The similar trend of Hall-Petch relation was reported by many researchers(Ref 38-40). The smaller grain structure is well connected with each other by higher interaction energy and adhesion. Each grain's connection has a higher contact area, which improves the crystallite bonding, and achieves improved adhesion. The grain boundary restricts the dislocation, which affects the strength of the material. The formation of grain size is also affected by residual stress and environmental conditions. However, larger grains attributed to the longer dislocation and

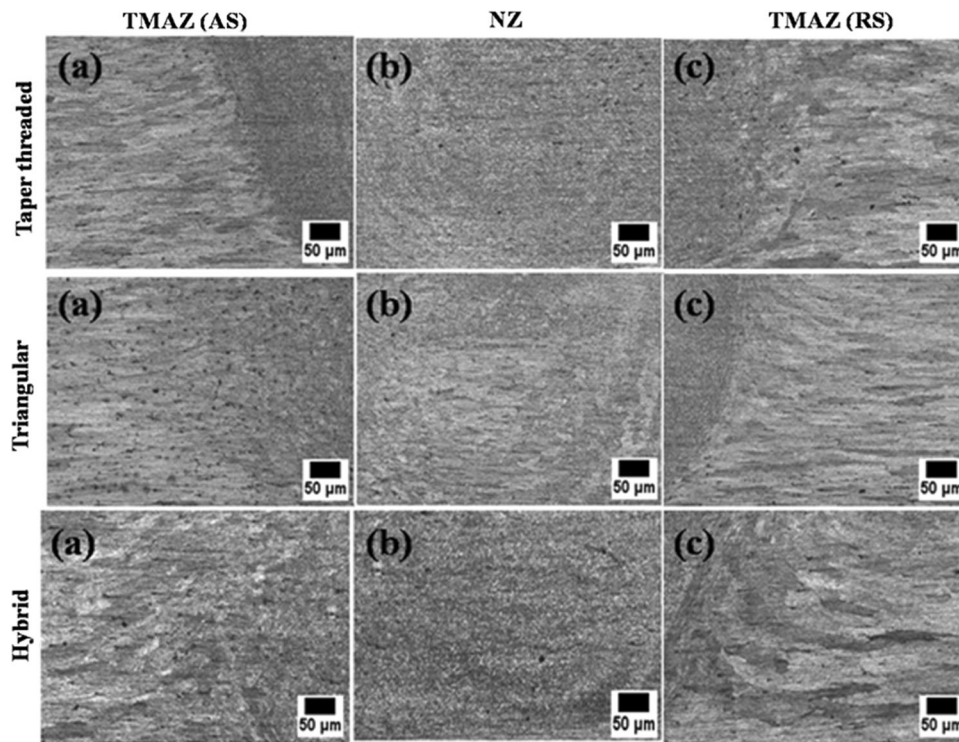


Fig. 4 Microstructure of the different tool pin profile at the different zone: (a) TMAZ-AS; (b) NZ and (c) TMAZ-RS

required lower stress to activate these dislocations (Ref 41). It indicates that the bigger crystal is weaker than, the smaller ones. The triangular pin profile showed a larger grain size ($17.62\ \mu\text{m}$), whereas the hybrid tool revealed a lower grain size ($11.27\ \mu\text{m}$) and is shown in Table 3. The reduction in the welded material's grain size improves the mechanical-properties of the sample (Ref 42).

The graph plotted between the grain size and counts in NZ with different tool pin profile is presented in Fig. 8. The Linear intercept method is attributed to measure the average grain diameter, according to ASTM E112-12. The smaller grain size population is evident in NZ by hybrid pin profile. The higher shear stress and decreased heat input may be the reason for the larger average grain size which was observed in triangular pin profile. The taper threaded tool pin profile, which has provided sufficient mixing by tool geometry (screw threaded) on same parameters. The counts increased with smaller grain size and decreased with an increase in larger grain size due to adequate mixing of the material, which provides higher strength.

4. Analysis of the Tensile Properties

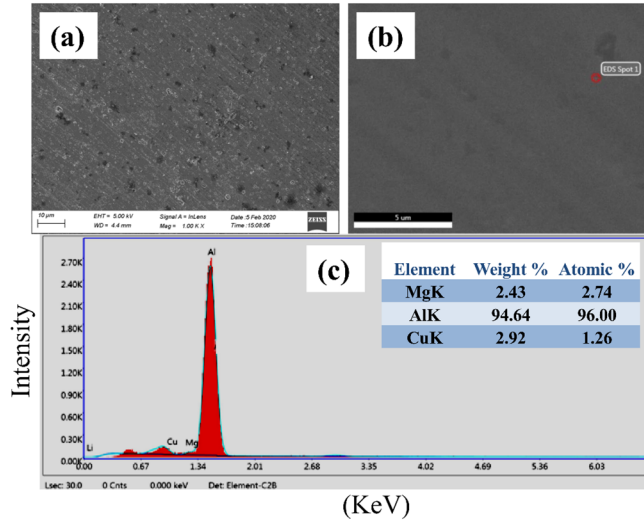
The tensile properties of the welded AA2050–T84 alloy by different tool pin profiles are discussed in this section. The tensile fracture location of the welded samples and their nature of failure mode by FE-SEM is discussed in this section.

4.1 Tensile Strength, Elongation(%) and Joint Efficiency Analysis

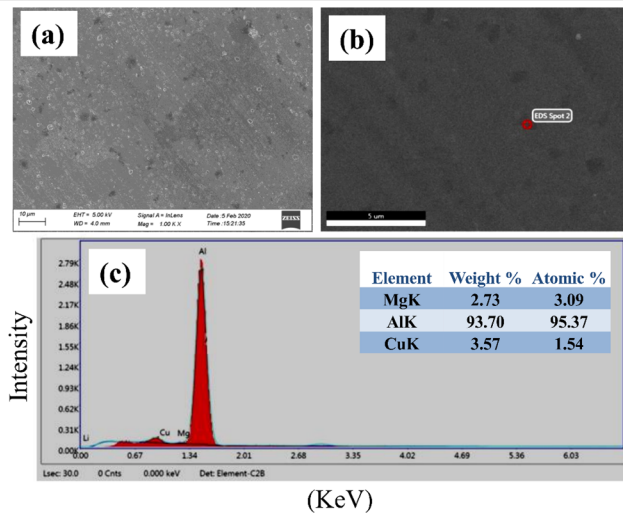
The tensile test of sliced welded samples was performed, and the strength of the joint was evaluated. Fig. 9 presents the tensile properties of all-welded samples with different pin

profile tools at constant TRS (1400 rpm), TTS (180 mm/min), and TTA (2°). It is worth noting that the highest value of tensile strength (TS), % elongation (%E), and joint efficiency (η) of the welded joint achieved by a hybrid tool pin profile was 418.98MPa, 10, and 78.44%, respectively, which is 27.47% lower than the base metal. The FSW joints fabricated using triangular tool pin profile yielded the lower TS, %E, and η of 298.17MPa, 3.51, and 55.8%. P. Goel et al. (Ref 43) welded AA6063 using different tools like tapered cylindrical, cylindrical, hexagonal, triangular and square. Higher joint efficiency (73.6%) was achieved through a tapered cylindrical tool. Suresh et al. (Ref 44) optimized parameters and joined AA7075 plates, using a conical tool and square tool, obtained higher efficiency (59.42%) through the square tool. Ma et al. (Ref 45) reported higher efficiency (74.5%) by using three groove pin tip among all tool (thread taper, triangular, square, three grooves, and conical tool). The FSW joint made by using the hybrid tool shows more joint efficiency when compared to the above-reported literature. The hybrid tool pin profile achieved the highest strength due to its pin structure, which exhibited larger swept volume and increased stirring power. The hybrid tool pin profile generated an appropriate magnitude of frictional heat during FSW, which was accountable for the excellent mixing of the material and flowed smoothly from the AS to RS. The triangular tool pin profile impeded the reduced heat generation and deformation of metal during FSW due to less interfacial contact between the tool probe and workpiece; results produced the welded joints with lower tensile properties. The elongation of tensile sample which was welded by hybrid tool is more when compared to the taper threaded tool. It may be due to amount of heat generation and tensile fracture position which strongly affects the elongation of welded sample. The generation of heat influences the plastic deformation of the material, molecular structure and tensile fracture position that ultimately affects the

(a) Triangular tool



(b) Taper threaded



(c) Hybrid

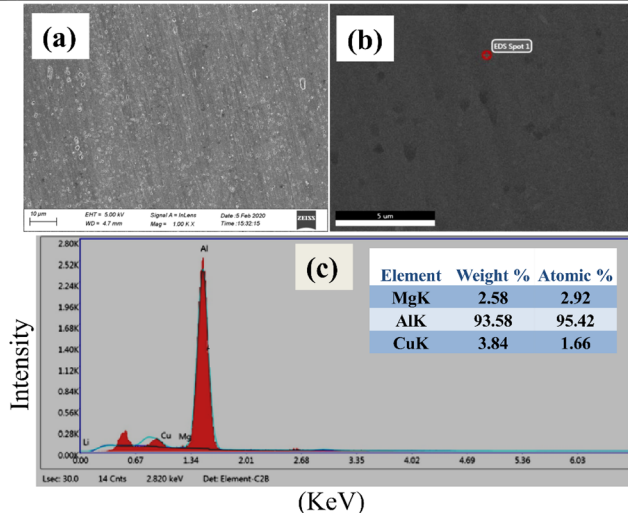


Fig. 5 SEM and EDS analysis of the welded sample by using different tool profile; (a) at the NZ (b) point EDS image of particle (c) EDS analysis and percentage elements composition on respective point

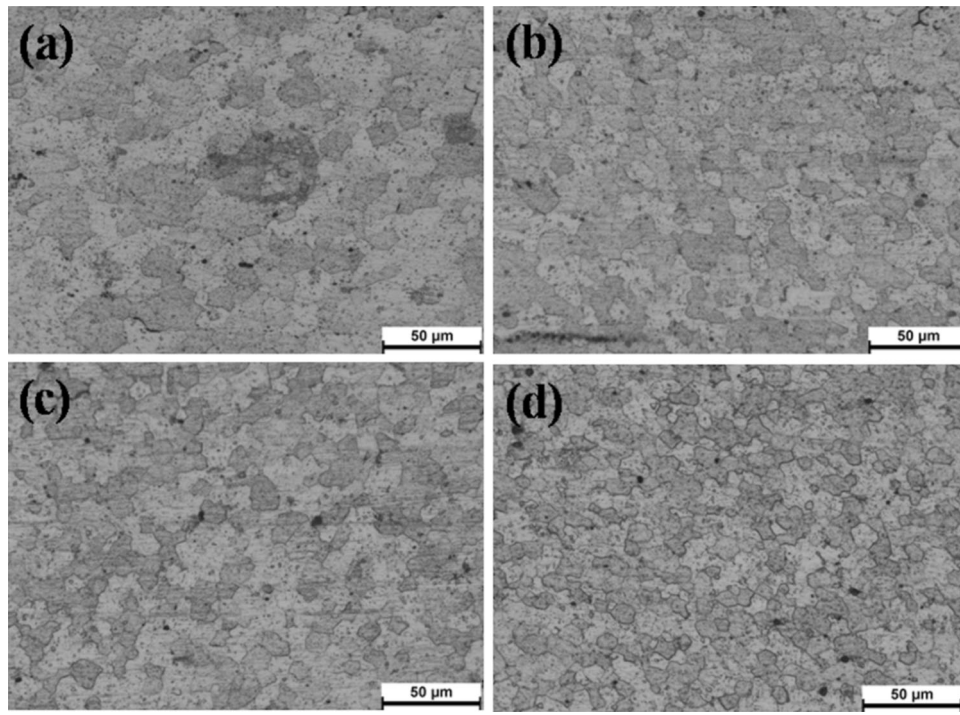


Fig. 6 Grain distribution in NZ of the different tool pin profile: (a) Triangular pin profile (b) Taper threaded pin profile (c) Bottom position (taper threaded end) of hybrid; and (d) End position (triangular end) of hybrid tool

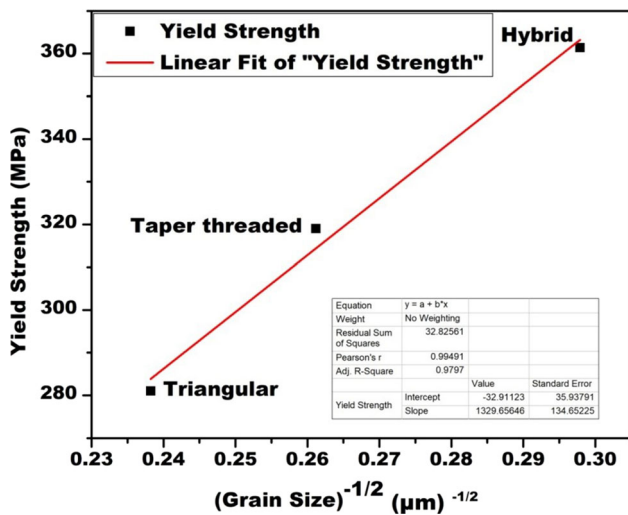


Fig. 7 Grain size of different tool pin profile with Yield strength

Table 3 Average grain size at the NZ welded with different tool profile

Tool Profile	NZ, μm
Triangular	17.62
Taper threaded	14.66
Hybrid	
Middle position (Taper threaded end)	13.46
End position (Triangular end)	11.27

tensile strength. The elongation also affected by the softening of the material around the weld. The tensile sample broke in NZ which was joined by hybrid tool whereas sample joined by taper threaded broke in TMAZ, and it is clearly shown in Fig. 11.

4.2 Hardness Analysis

The hardness of a welded samples are significantly influenced by different tool pin profiles. Figure 10 shows the comparison of micro-hardness distribution patterns over the welded joint's mid-thickness in the traverse direction produced by incorporating varying tool pin profiles. The hardness profile of the welded specimen by using different tool pin profiles has the same characteristic (i.e., W-shaped) at constant TRS, TTS, and TTA. The hardness of the weld nugget varies according to the tool pin profiles and it is found to be lower than the base material that lies between the range of 170-175HV_{0.1}. HTP revealed the maximum hardness value (147HV_{0.1}). However, a lower hardness value (138HV_{0.1}) was observed by the triangular tool pin. The grain size of the welded specimen is affected by the heat input which was provided by the different tool pins during FSW. The grain size of the welded specimen is affected by the heat input which was provided by the different tool pins during FSW and according to the Hall–Petch relation, the grain size is the inverse square root of the hardness. In the current investigation, a similar observation was made (the triangular tool produced larger grain size (17.62 μm) in NZ but lower hardness value, whereas, a HTP generated smaller grain size (12.01 μm) with a higher hardness value). It may be possible that the better plasticized material flow is related to the hybrid tool's ability to generate a significant quantity of heat during FSW. TMAZ has the lowest hardness value compared to the other zones, as illustrated in Fig. 10.

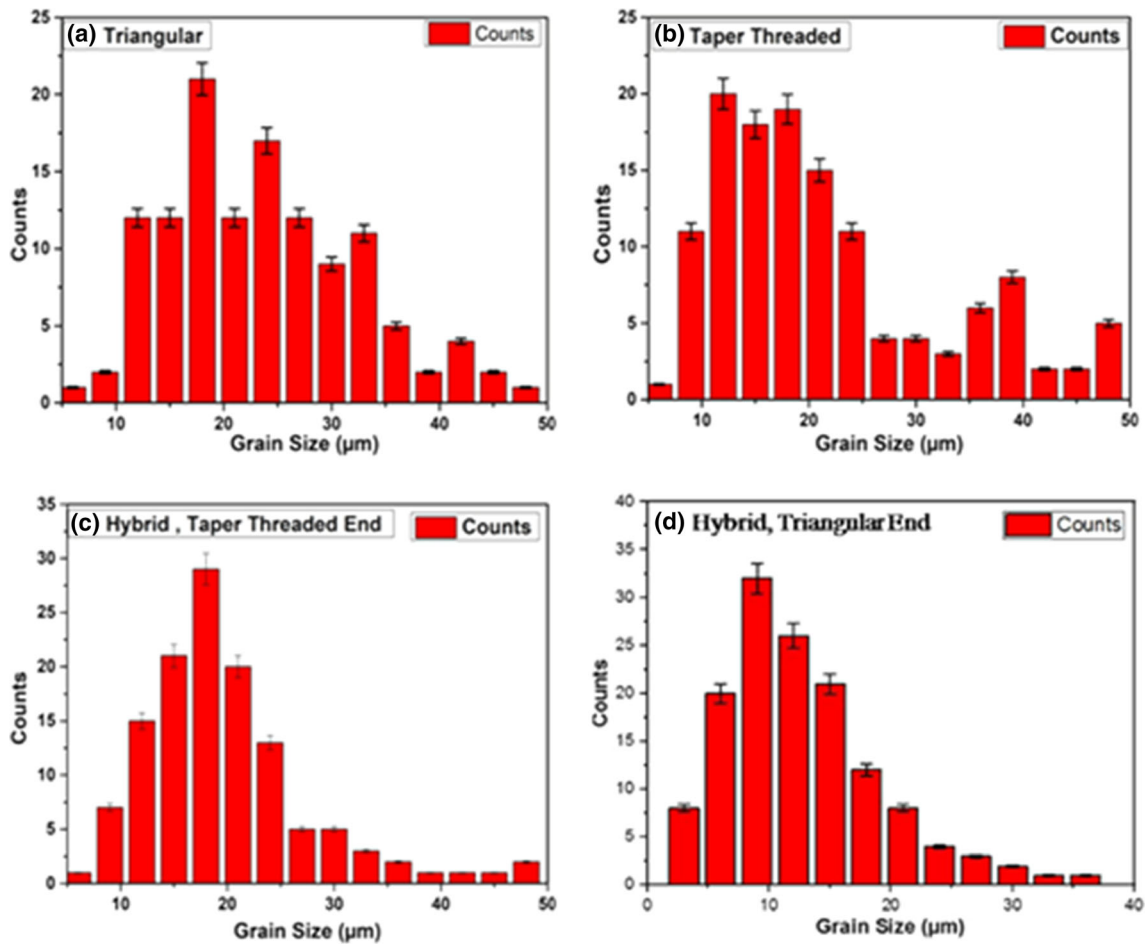


Fig. 8 Grain distribution in NZ with different tool pin profile

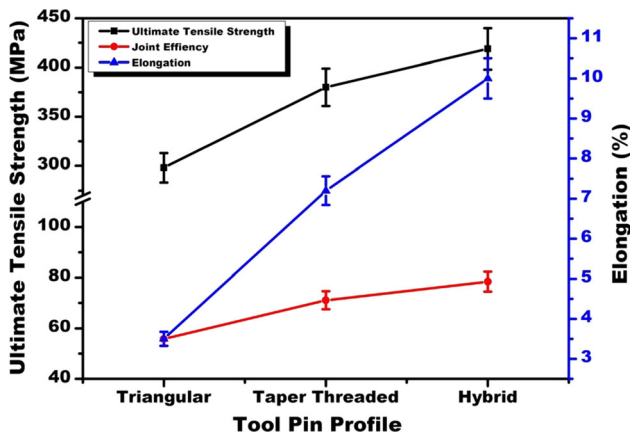


Fig. 9 Tensile properties of the welded sample using different tool pin profile

4.3 Fractography Analysis

The fracture features of tensile fracture surfaces with different tool pin profile are incorporated in present study. The tensile mode of failure has been carried out by the SEM image, shown through the enlarged view of the inferior surface, and is depicted in Fig. 11. The tensile fracture is visible in different ways using different tool profiles due to the induced stress concentration during the tensile test. This failure of the

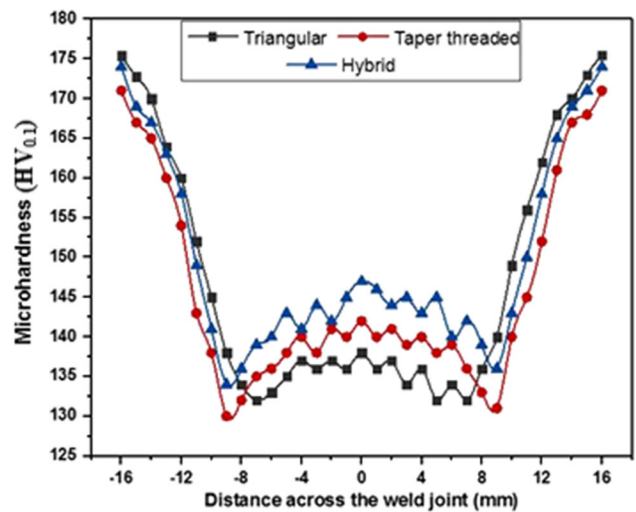


Fig. 10 Micro-hardness distribution profile across the weld region for 2050-T84 Al-Cu-Li alloy using different tool pin profile

tensile fracture surface propagated from NZ and moved toward TMAZ, and the region of crack initiation was the weakest region formed among whole crack. The formation of a cup-cone-type of structure and dimple is seen in the sample welded by the triangular pin, indicating the fracture surface's flexible nature. The tear ridge is also found on the fracture surface, as

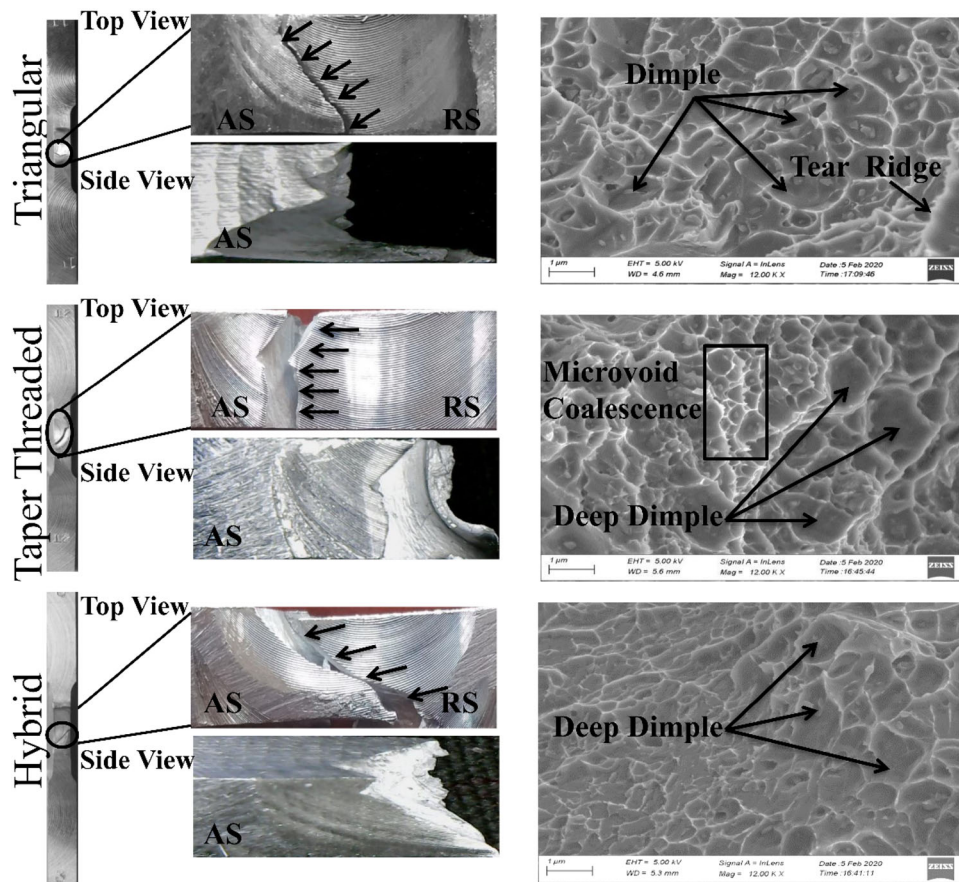


Fig. 11 Fracture morphology of friction stir welded samples using the different tool pin profile

depicted in the SEM image. The presence of coalescence of microvoid proceeds to the formation of dimple, giving it a fibrous appearance due to the deformation of the material and hence proceed in ductility of tensile fracture sample. The tensile sample of the material welded by a taper threaded tool pin shows a sharper edge formed on the weld bead surface, which can be easily seen. The sharp edge plastically deformed the material in NZ and TMAZ, which may be due to the deformation material's variance in NZ and TMAZ. A cone-type fracture was seen in AS of the broken tensile specimen with a taper threaded tool pin. The deep dimple and microvoid coalescence appeared on the fracture surface with a higher magnification image of SEM, which designates ductility fracture. However, in the hybrid tool, the population of the alike dimple was observed in the fracture surface with higher magnification, indicating ductile fracture mode. The fracture has been observed in NZ by using hybrid tool.

5. Conclusions

In this study, a 5mm thick 2050-T84 Al-Cu-Li alloy was fabricated by friction stir-welding using varying tool pin profile, namely taper threaded, triangular, and novel hybrid tool pin at constant TRS, TTS, and TTA. Optimum TRS, TTS, and TTA were maintained through the trial and error method, which provide sound weld joint and improved mechanical

properties. The relevant conclusion can be drawn based on the present study, which is as follows:

- Novel hybrid tool pin profile is introduced in the present study, which is the coupling of the taper threaded and triangular tool pin.
- Less fluctuation was observed in force and torque behavior using a hybrid tool compared to a taper threaded and triangular tool pin.
- Minimum average X-Force (2053.83 N), Z-Force (14340.49 N), and little bit high torque (10.99Nm) were incorporated by the hybrid tool, however maximum by the triangular tool if the tool pin were not broken.
- The hybrid tool produced more smooth weld and provided a large weld nugget area (33.95 mm²) and generate high heat input 536.8 J/mm among all tools due to dynamic recrystallization and plastic deformation during FSW.
- The equiaxed and finer grain size (11.27 μm) was observed at NZ in a hybrid tool; however, the larger grain size was observed in the triangular tool pin (17.62 μm).
- The maximum tensile strength (418.98 MPa) and joint efficiency (78.44%) were observed by the hybrid tool. However, minimum tensile strength (298.17MPa) and joint efficiency (55.8%) was revealed by the triangular tool pin.
- The maximum hardness value (147HV_{0.1}) is observed by HTP. However lower hardness value is found (138HV_{0.1}) by triangular tool pin profile.

Acknowledgment

The authors acknowledge financial assistance in terms of scholarship to carry the research work from the Ministry of Human Resource and Development (MHRD), Government of India. The authors also acknowledge the Mechanical Engineering Department, IIT Guwahati, India (for providing the facilities of Material Testing of the welded specimen), and Tripura University (for FE-SEM analysis of tensile fracture specimen).

Conflict of interest

The author has no conflict of interest.

References

1. R. Bertrand, H. Robe, D. Texier, Y. Zedan, E. Feulvarch and P. Bocher, Analysis of AA2XXX/ AA7XXX Friction Stir Welds, *J. Mater. Process Technol.*, 2019, **271**, p 312–324.
2. B. Ahmed and S. Wu, Aluminum-Lithium Alloys (Al-Li-Cu-X)-New Generation Material for Aerospace Applications, *Appl. Mech. Mater.*, 2013, **440**, p 104–111.
3. S. Kumar, D. Sethi, S. Choudhury, B.S. Roy and S.C. Saha, An Experimental Investigation to the Influence of Traverse Speed on Microstructure and Mechanical Properties of Friction Stir Welded AA2050-T84 Al-Cu-Li Alloy Plates, *Mater. Today*, 2020, **26**(2), p 2062–2068.
4. J. Zhang, X.S. Feng, J.S. Gao, H. Huang, Z.Q. Ma and L.J. Guo, Effects of Welding Parameters and Post-Heat Treatment on Mechanical Properties of Friction Stir Welded AA2195-T8 Al-Li Alloy, *J. Mater. Sci. Technol.*, 2018, **34**, p 219–227.
5. M. Niedzinski, The Evolution of Constellium Al-Li alloy for Space Launch and Crew Module Application, *Light. Met. Age*, 2019, **77**, p 36–42.
6. A.A. El-Aty, Y. Xu, X. Guo, S. Zhang, Y. Ma and D. Chen, Strengthening Mechanisms, Deformation Behavior, and Anisotropic Mechanical Properties of Al-Li Alloys: A Review, *J. Adv. Res.*, 2018, **10**, p 49–67.
7. O. Gharbi, N. Birbilis and K. Ogle, Li Reactivity During The Surface Pretreatment of Al-Li Alloy AA2050-T3, *Electrochim. Acta.*, 2017, **243**, p 207–219.
8. R.J.H. Wanhill, and G.H. Bray, Aero-Structural Design and its Application to Aluminum-Lithium Alloys. In Aluminum-Lithium Alloys: Processing, Properties, and Applications. Prasad E, Gokhale A, and Wanhill H, editors: Butterworth-Heinemann; Elsevier Inc; 2014; p 27–58
9. Ph. Lequeu, K.P. Smith and A. Daniélou, Aluminum-Copper-Lithium Alloy 2050 Developed for Medium to Thick Plate, *J. Mater. Eng. Perform.*, 2009, **19**, p 841–847.
10. S. Kumar, U. Acharya, D. Sethi, T. Medhi, B.S. Roy and S.C. Saha, Effect of Traverse Speed on Microstructure and Mechanical Properties of Friction Stir Welded Third Generation Al-Li Alloy, *J. Braz. Soc. Mech. Sci. Eng.*, 2020, **42**(423), p 1–13.
11. V. Proton, J. Alexis, E. Andrieu, C. Blanc, J. Delfosse, L. Lacroix and G. Odemer, Influence of Post-Welding Heat Treatment on the Corrosion Behavior of a 2050-T3 Aluminum-Copper-Lithium Alloy Friction Stir Welding Joint, *J. Electrochem. Soc.*, 2011, **158**(5), p 39–147.
12. M.N. Avettand-Fènoël, F. DeGeuser and A. Deschamps, Effect of the Aging on Precipitation Spatial Distribution in Stationary Shoulder Friction Stir Welded AA2050 Alloy, *Mater. Charact.*, 2019, **154**, p 193–199.
13. B. Cai, Z.Q. Zheng, D.Q. He, S.C. Li and H.P. Li, Friction Stir Weld of 2060 Al-Cu-Li Alloy: Microstructure and Mechanical Properties, *J. Alloys Compd.*, 2015, **649**, p 19–27.
14. R.S. Mishra and H. Sidhar, *Friction Stir Welding of Al-Li Alloys. Chapter-4, Friction Stir Welding of 2XXX Aluminum Alloys Including Al-Li Alloys*, Butterworth-Heinemann, Oxford, 2017
15. W.M. Thomas, D.G. Staines, I.M. Norris and R. de Frias, Friction Stir Welding Tools and Developments, *Weld. World.*, 2003, **47**, p 10–17.
16. L. Shi and C.S. Wu, Transient Model of Heat Transfer and Material Flow at Different Stages of Friction Stir Welding Process, *J. Mater. Process*, 2017, **25**, p 323–339.
17. Y.N. Zhang, X. Cao, S. Larose and P. Wanjara, Review of Tools for Friction Stir Welding and Processing, *Can. J. Metall. Mater. Sci.*, 2013, **51**(3), p 250–261.
18. J. Stephen Leon and V. Jayakumar, Effect of Tool Shoulder and Pin Cone Angles in Friction Stir Welding using Non-Circular Tool Pin, *J. Appl. Comput. Mech.*, 2020, **6**(3), p 554–563.
19. S. Ugender, Influence of Tool Pin Profile and Rotational Speed on the Formation Of Friction Stir Welding Zone in AZ31 Magnesium Alloy, *J Magns Alloy*, 2018, **6**(2), p 205–213.
20. Y. Birol and S. Kasman, Effect of Welding Parameters on Microstructure and Mechanical Properties of Friction Stir Welded EN AW 5083 H111 Plates, *Mater. Sci. Tech.*, 2013, **29**(11), p 1354–1362.
21. K. Elangovan, V. Balasubramanian and M. Valliappan, Influences of Tool Pin Profile and Axial Force on the Formation of Friction Stir Processing Zone in AA6061 Aluminum Alloy, *Int. J. Adv. Manuf. Tech.*, 2007, **38**(3–4), p 285–295.
22. R. Palanivel, P. Koshy Mathews, M. Balakrishnan, I. Dinaharan and N. Murugan, Effect of Tool Pin Profile and Axial Force on Tensile Behavior in Friction Stir Welding of Dissimilar Aluminum Alloys, *Adv. Mater. Res.*, 2012, **415**, p 1140–1146.
23. S Budin, N C Maideen and S Sahudin (2019) Design and Development of Stirring Tool Pin Profile for Reconfigured Milling Machine to Perform Friction Stir Welding Process. In IOP Conference Series: Mater. Sci. Engg. 505: 012089
24. Ch. VenkataRao, G. Madhusudhan Reddy and K. SrinivasaRao, Influence of Tool Pin Profile on Microstructure and Corrosion Behavior Of Aa2219 Al-Cu Alloy Friction Stir Weld Nuggets, *Def Tech.*, 2015, **11**(3), p 197–208.
25. M.M. Moradi, H.J. Aval and R. Jamaati, Effect of Tool Pin Geometry and Weld Pass Number on Microstructural, Natural Aging And Mechanical Behavior of SiC-Incorporated Dissimilar Friction-Stir-Welded Aluminium Alloys, *Sādhanā.*, 2019, **44**(9), p 1–9.
26. A. Singh, V. Kumar and N.K. Grover, Influence of Tool Pin Profiles on Friction Stir Welding With a Gap for AA6082-T6 Aluminum Alloy, *Mater. Res. Expr.*, 2019, **6**(8), p 8.
27. K. Elangovan, V. Balasubramanian and M. Valliappan, Effect of Tool Pin Profile and Tool Rotational Speed on Mechanical Properties of Friction Stir Welded AA6061 Aluminium Alloy, *Mater. Manuf. Process.*, 2008, **23**(3), p 251–260.
28. B. Singh, K.K. Saxena, P. Singhal and T.C. Joshi, Role of Various Tool Pin Profiles in Friction Stir Welding of AA2024 Alloys, *J Mater Eng Perform*, 2021 <https://doi.org/10.1007/s11665-021-06017-3>
29. H.I. Dawood, K.S. Mohammed, R. Azmi and M.B. Uday, Effect of small Tool Pin Profiles on Microstructures And Mechanical Properties Of 6061 Aluminum Alloy by Friction Stir Welding, *T Non Ferr. Metals Soc.*, 2015, **25**(9), p 2856–2865.
30. M. Shalin and M. Hiten, Experimental Analysis on Effect of Tool Transverse Feed, Tool Rotational Speed And Tool Pin Profile Type on Weld Tensile Strength OF Friction Stir Welded Joint of AA 6061, *Mater Today: Proce*, 2018, **5**(1), p 487–493.
31. D.B. Darmadi and M. Talice, Improving the Strength of Friction Stir Welded Joint By Double Side Friction Welding and Varying Pin Geometry, *Eng. Sci. Technol. Int. J.*, 2021, **24**(3), p 637–647.
32. J.C. Hou, H.J. Liu and Y.Q. Zhao, Influences of Rotation Speed on Microstructures and Mechanical Properties of 6061-T6 Aluminum Alloy Joints Fabricated by Self-Reacting Friction Stir Welding Tool, *Int. J. Adv. Manuf. Tech.*, 2014, **73**(5–8), p 1073–1079.
33. M.M. Khalilabad, Y. Zedan, D. Texier, M. Jahazi and P. Bocher, Effect of Tool Geometry and Welding Speed on Mechanical Properties of Dissimilar AA2198-AA2024 FSWed Joint, *J. Manuf. Process.*, 2018, **34**, p 86–95.
34. M Guerra, CSchmidt, J. C. McClure, L. E. Murr, A. C. Nunes, and P. M. Munafo, Metal Flow during Friction Stir Welding, in Friction Stir Welding and Processing, K. V. Jata, R. S. Mishra, S. L. Semiatin, D. P. Field, Editor, 2001, TMS Indianapolis, Indiana, p. 246
35. A. Tongne, C. Desrayaud, M. Jahazi and E. Feulvarch, On Material Flow in Friction Stir Welded Al alloys, *J. Mater. Proc. Tech.*, 2017, **239**, p 284–296.
36. Y.S. Sato, M. Urata, H. Kokawa and K. Ikeda, Hall-Petch Relationship in Friction Stir Welds of Equal Channel Angular-Pressed Aluminum Alloys, *Mater. Sci. Eng. A*, 2003, **354**(1–2), p 298–305.
37. C. Du, Q. Pan, S. Chen and S. Tian, Effect of Rolling on the Microstructure And Mechanical Properties Of the T DS-FSW Plate, *Mater. Sci. Eng.: A*, 2019, **138692**, p 1–24.

38. A. Jagetia, M.S.K.K.Y. Nartu, S. Dasari, A. Sharma, B. Gwalani and R. Banerjee, Ordering-Mediated Local Nano-Clustering Results in Unusually Large Hall-Petch Strengthening Coefficients in High Entropy Alloys, *Mater. Res. Lett.*, 2019, **5**, p 213–222.
39. Y. Li, A.J. Bushby and D.J. Dunstan, The Hall-Petch Effect as a Manifestation of the General Size Effect, *Proc. R. Soc. A: Math., Phys. Eng. Sci.*, 2016, **472**(2190), p 20150890.
40. L. Chun-Yi, L. Truan-Sheng, C. Li-Hui and H. Fei-Yi, Hall Petch Tensile Yield Stress and Grain Size Relation of Al5Mg05Mn Alloy in Friction-Stir-Processed and Post-Thermal-Exposed Conditions, *Mater. Trans.*, 2014, **55**(2), p 357–362.
41. N. Guo and M.C. Leu, Additive Manufacturing: Technology, Applications, and Research Needs, *Front. Mech. Eng. Proc.*, 2013, **8**(3), p 215–243.
42. P. Schempp, C.E. Cross, R. Häcker and M.R. Ethmeier, Influence of Grain Size on Mechanical Properties of Aluminum GTA Weld Metal, *Weld. World.*, 2013, **57**(3), p 293–304.
43. P. Goel, A.N. Siddiquee, N.Z. Khan, A. Mohd, Z.A. Hussain, M.H. Khan and A. Al-Ahmari Abidi, Investigation on the Effect of Tool Pin Profiles on Mechanical and Microstructural Properties of Friction Stir Butt And Scarf Welded Aluminium Alloy 6063, *Metals*, 2018, **8**, p 74.
44. C.N. Suresha, B.M. Rajaprakash and S. Upadhya, A Study Of The Effect of Tool Pin Profiles on Tensile Strength of Welded Joints Produced Using Friction Stir Welding Process, *Mater. Manuf. Proc.*, 2011, **26**(9), p 1111–1116.
45. M. Yuqing, K. Liming, L. Fencheng, C. Yuhua and X. Li, Effect of Tool Pin-Tip Profiles on Material Flow and Mechanical Properties of Friction Stir Welding Thick AA7075-T6 Alloy Joints, *Int J Adv Manuf Technol*, 2017, **88**, p 949–960.

Publisher's Note Springer Nature remains neutral with regard to jurisdictional claims in published maps and institutional affiliations.